Radiation damage formation in InP, InSb, GaAs, GaP, Ge, and Si due to fast ions

A. Kamarou,* W. Wesch, and E. Wendler
Institut für Festkörperphysik, Friedrich Schiller Universität Jena, Max-Wien-Platz 1, D-07743 Jena, Germany†

A. Undisz and M. Rettenmayr
Institut für Materialwissenschaft und Werkstofftechnologie, Friedrich Schiller Universität Jena, Löbdergraben 32, D-07743 Jena, Germany

(Received 21 April 2008; revised manuscript received 15 July 2008; published 15 August 2008)

The basic physical mechanisms of damage formation in semiconductors due to swift heavy ion (SHI) irradiation are not yet fully understood. In the present paper damage evolution and the formation of ion tracks during SHI irradiation in InP, InSb, GaAs, GaP, and Ge are investigated for irradiation with Xe or Au ions having specific energies ranging from about 0.8 to 3 MeV/u. Based on these experimental results and those obtained by other authors for cluster-ion irradiation of InP, GaAs, Ge, and Si, extensive calculations were performed in the framework of the thermal spike model. As we published previously, the model was extended to correctly treat processes being specific to semiconductors. Additionally, the computer code was modified to perform calculations for cluster ions too. The calculated track radii are compared with those measured for the various irradiation conditions. Thereby, one unknown parameter in the calculations was determined by fitting *one* data point. With this procedure a very good agreement between calculated and measured track radii is obtained for InP, Ge, and Si irradiated under *various* conditions. This implies that the extended thermal spike model is well capable to explain track formation in SHI irradiated semiconductors. Furthermore, special experiments were performed, the results of which also support the thermal spike model of ion track formation and contradict competing mechanisms such as Coulomb explosion, shock waves, or lattice relaxation. Thus, visible (amorphous/heavily damaged) ion tracks occur if the electronic energy deposition per ion and unit length clearly exceeds the threshold value necessary for melting. This is possible for elemental ion irradiation of InP and InSb. In Ge and Si (and probably also in GaAs and GaP) the energy deposition necessary for melting is that high that it cannot be reached by elemental ion irradiation. Moreover, at least in InP and GaAs ion tracks can be formed also in a subthreshold irradiation regime if the material is *predamaged*. This suggests that the existence of point defects and clusters of point defects in the crystal lattice noticeably increases the electron-phonon coupling efficiency, resulting in a more efficient energy transfer to the lattice. Within the thermal spike model, this means that for a given electronic energy deposition in the predamaged crystal a higher temperature is reached than in the perfect one.

DOI: 10.1103/PhysRevB.78.054111 PACS number(s): 61.72.Cc, 61.80.Jh, 61.82.Fk, 81.05.Ea

I. INTRODUCTION

In the last decades ion implantation into solids has evolved into a powerful and well established technique widely used to modify various physical properties of materials in locally defined regions. In particular, irradiation of solids with very fast projectiles (having energies within the megaelectron volt or even gigaelectron volt range) leads to many spectacular effects not specific to irradiations with much less energetic ions. To study the effect of fast ion bombardment on structural modification in various materials is thus not only of interest for the formation of nanotubes within the target matrix, for instance, but also in connection with the use of semiconductor devices under extreme conditions, as, e.g., in space or in the vicinity of particle accelerators or nuclear reactors.

Four main competing mechanisms of the damage formation in solids due to high electronic energy deposition are discussed in literature. These are Coulomb explosion,[1–4] shock waves,[5–7] lattice relaxation (also called "athermal melting"),[8–10] and inelastic thermal spikes[11–15] dating back to Dessauer,[16] and Seitz and Koehler.[17] Due to the complexity of all energy relaxation processes involved, all four models are subjected to criticism. However, among them the thermal spike model seems to be the most elaborated one; furthermore, currently it is the only model being able to provide at least approximate predictions on ion track formation in numerous conducting and nonconducting targets.

The thermal spike model suggests that the electronic energy is transferred to the lattice via various processes of electron-phonon coupling, which leads to an increase in the lattice temperature. If this increase surpasses the melting point, the material can melt and the following fast cooling down of the molten zone can freeze the resulting damage in and thus leave an ion track behind.

No experimental results available in literature directly prove that a fast heavy ion passing through matter causes a local melting of the target material at the ion path and close to it. As a rule, the resulting effects (e.g., various phase transformations in simple or layered structures, or modifications of the existing surfaces and interfaces, etc.) are registered and measured on a time scale that is incommensurable with the characteristic time intervals of the basic processes being the first cause of the changes observed. (The "microscopical" or "nanoscale" processes triggered by a fast ion penetrating the matter usually do not last longer than 10^{-13} to 10^{-10} s, whereas the conventional methods, such as Rutherford backscattering spectrometry (RBS), transmission electron micros-

TABLE I. Selected basic and thermal properties of InP, InSb, GaAs, GaP, Ge, and Si at 300 K.

Property/material	InP	InSb	GaAs	GaP	Ge	Si
Structure	Zinc blende	Zinc blende	Zinc blende	Zinc blende	Diamond	Diamond
Space group	$F\bar{4}3m$	$F\bar{4}3m$	$F\bar{4}3m$	$F\bar{4}3m$	$Fd3m$	$Fd3m$
Lattice parameter a_0 (nm)	0.587	0.648	0.565	0.545	0.566	0.543
Mass density (solid) ρ_s (g/cm^3)	4.79	5.77	5.32	4.13	5.32	2.33
Mass density (liquid) ρ_l (g/cm^3)	5.1	6.46	5.71	4.6	5.6	2.57
Atomic density N_a (10^{22} cm^{-3})	3.96	2.94	4.42	4.94	4.40	5.00
Nature of energy gap	Direct	Direct	Direct	Indirect	Indirect	Indirect
Energy gap E_g (eV)	1.34	0.17	1.42	2.27	0.66	1.12
Thermal conductivity [W/(m K)]	72	18	55	110	58	148
Specific heat C_p [J/(g K)]	0.31	0.20	0.33	0.43	0.31	0.65
Melting point T_m (K)	1335	800	1513	1730	1210	1683

copy (TEM), secondary-ion-mass spectrometry (SIMS), optical ones, etc., demand many orders of magnitude larger time spans for collecting a spectrum or acquiring an image even if applied *in situ*.

Nevertheless, some observed effects support the idea of the local melting indirectly. One of such effects is the well-known intermixing in layered structures by swift heavy ions (SHIs).[18–24] It was shown that the mixing takes place only if the electronic energy deposition per unit length, ε_e, exceeds a certain threshold value (above threshold regime) that is determined by the more radiation resistant material of the corresponding structure.[18] The last conclusion gives a clear indication that an efficient intermixing occurs only if both sides of the interface are locally molten by SHIs. Furthermore, for all experimental conditions favoring the intermixing (its efficiency is primarily dependent on the ion energy loss and on the irradiation temperature) the effect is governed by very efficient interdiffusion of the constituent atoms.[22,23] This diffusion is too fast to be ascribed to solid-state processes, because the respective diffusion coefficients (from about 10^{-4} to 10^{-2} cm^2 s^{-1}) are several orders of magnitude larger than the solid-state ones. In fact, such diffusion coefficients are characteristic to *liquid state diffusion*, which supports again the idea that the interface mixing results from the transient interdiffusion in the molten tracks of the SHIs.[25]

In this paper we present experimental and theoretical results on the formation and accumulation of radiation damage in various semiconductors due to fast heavy ions. Furthermore, one of the main purposes of this study was to check whether local melting of the target material within the tracks of fast ions occurs, and thus to determine which of the four mechanisms of the damage formation mentioned above is responsible for the track formation in the studied materials.

II. EXPERIMENTS

We have used ⟨100⟩-oriented single crystalline mirror polished wafers of InP, InSb, GaAs, GaP, and Ge bought from the CrysTec company. All wafers were nominally undoped. Only in the case of InP some of the samples were doped with S or Cd during the crystal growth resulting in *n* or *p* doping of the substrate, respectively. Some selected basic and thermal properties of the investigated materials are presented in Table I. The table data are from Refs. 26–30. The wafers were cut into pieces (typically from 5×5 to 8×8 mm^2 large), and the samples were then irradiated at the Hahn-Meitner-Institut with 390 $^{129}Xe^{21+}$ or 593 MeV $^{197}Au^{30+}$ ion beams either at room temperature (RT) or at liquid nitrogen temperature (LNT) (77 K). The irradiation conditions are briefly outlined in Table II. Ion-beam scanning was used to irradiate the whole sample surface in a uniform way. In order to prevent heating of the samples during the irradiations, the samples were mounted to the sample holder with silver paste giving a good thermal contact between them. Additionally, 0.8 μm thick aluminum (Al) foils were placed in front of some samples to bring the projectiles into the mean equilibrium charge state. As follows from the SRIM-2003 calculations,[31] in this way the fast Xe and Au ions mentioned above were decelerated by about 15 and 20 MeV, respectively, resulting in 375 MeV Xe and 573 MeV Au beams. Several samples of InP were also irradiated with 593 MeV Au ions through a 20 μm thick Al foil resulting in a 150 MeV Au ion beam. Furthermore, in order to check whether existing lattice disorder has influence on the radiation damage formation, some GaAs samples were predamaged prior to the SHI irradiations. The predamaging was performed by means of implantation of 600 keV Ge ions at LNT. The respective calculations with the SRIM-2003 code[31] show that the predamaged layers reach depths not larger than 500 nm.

In order to analyze the samples, mainly three experimental methods were used: Rutherford backscattering spectrometry combined with the channeling technique (RBS/Ch), TEM, and SIMS. As a measure of the relative concentration of damage within the irradiated layers, the difference in minimum yield $\Delta\chi_{\min}$ was taken. It is determined from the channeling RBS spectra as a function of the depth z by $\Delta\chi_{\min}(z)=\frac{Y_{\text{aligned}}^{\text{irradiated}}(z)-Y_{\text{aligned}}^{\text{virgin}}(z)}{Y_{\text{random}}(z)-Y_{\text{aligned}}^{\text{virgin}}(z)}$, where $Y_{\text{aligned}}^{\text{virgin}}(z)$ and $Y_{\text{aligned}}^{\text{irradiated}}(z)$ are the RBS yields of the aligned spectra (unirradiated virgin and irradiated samples, respectively); $Y_{\text{random}}(z)$ is the yield measured in random direction. Assuming a random distribution of displaced lattice atoms within the lattice cell, the depth distributions of the relative concentration of displaced

TABLE II. Performed fast ion irradiations. Ion energy E, range of ion fluences N_I, irradiation temperature T_I, electronic (ε_e) and nuclear (ε_n) energy loss, and number of displacements N_d per ion and unit path length. The values of ε_e, ε_n, and N_d were calculated with the SRIM-2003 (Ref. 31) using mean displacement energies E_d of 8.0 eV for InP (Ref. 32), 7 eV for InSb (Ref. 33), 9.5 eV for GaAs (Ref. 34), 16.5 eV for GaP (Ref. 35), and 20 eV for Ge (Ref. 36).

Material	Ion	E (MeV)	N_I (cm^{-2})	T_I	ε_e (keV/nm)	ε_n (keV/nm)	N_d (nm^{-1})
	Xe	375	8.4×10^{11}	RT	21.4	0.046	1.5
	Xe	390	3×10^{11}–3×10^{14}	RT, LNT	21.5	0.044	1.4
InP	Au	150	5×10^{11}–2×10^{12}	RT	18.8	0.275	7.5
	Au	573	1×10^{11}	RT	28.9	0.082	2.6
	Au	593	1×10^{11}–1×10^{13}	RT	29.1	0.078	2.5
InSb	Au	573	5×10^{10}–5×10^{11}	RT, LNT	30.2	0.103	4.3
	Au	593	5×10^{10}–5×10^{11}	RT	30.4	0.100	4.2
GaAs	Au	573	5×10^{10}–1×10^{12}	RT, LNT	33.2	0.095	3.5
	Au	593	1×10^{13}–3×10^{14}	RT	33.3	0.091	3.4
GaP	Au	573	1×10^{12}	RT	29.1	0.082	1.3
	Au	593	8×10^{11}–5×10^{14}	RT	29.3	0.079	1.2
Ge	Au	593	5×10^{11}–3×10^{14}	RT	32.8	0.105	1.5

lattice atoms, $n_{da}(z)$, were calculated from the measured $\Delta\chi_{min}(z)$ values. These calculations were performed using the DICADA code[37] that is based on the discontinuous model of dechanneling. In the following the relative concentration of displaced lattice atoms, $n_{da}(z)$, is referred to as "damage concentration" for short. In all cases the values of n_{da} reported in this paper correspond to a depth of 200 nm.

Furthermore, some samples selected on the basis of the RBS results were additionally studied using TEM. The TEM investigations were performed using a JEOL JEM 3010 instrument operating at 300 kV. The thinned (electronically transparent) samples for TEM were prepared by means of chemical etching performed prior to SHI irradiations. The etching technique used saves much time and effort so as to allow thinning of many samples simultaneously; furthermore, it makes unnecessary such common steps as mechanical polishing and final ion-beam milling.

In order to prove whether fast heavy ion irradiation of semiconductors leads to local melting of the target material, we performed SIMS studies of the intermixing of layered structures. As already mentioned in Sec. I, such experiments are potentially capable to provide important information on the local melting of the target matter inside the ion tracks. For that purpose, two GaAs and InP samples were covered with thin (tens of nanometer) metallic surface layers by means of vapor deposition. Because the respective threshold (minimum) value of ε_e to trigger the intermixing is determined by the less sensitive material,[18] it is reasonable to select a material with a low radiation resistance. According to Refs. 38–40, such metals as Ti, Fe, Co, Zr, and Bi are the most sensitive ones with regard to fast ion irradiation. Therefore, they are the best candidates. Taking further into account the respective melting points (Ti: 1933 K, Fe: 1808 K, Co: 1768 K, Zr: 2125 K, and Bi: 545 K), Bi seems to be the best choice. Therefore, we prepared Bi/GaAs and Bi/InP layered structures by means of vapor deposition of Bi onto the GaAs or InP substrates, respectively. Afterwards, they were irradiated with 593 MeV Au ions up to a fluence of 5×10^{13} cm^{-2} at RT. Finally, both the unirradiated and SHI irradiated layered structures were investigated by means of SIMS. The SIMS studies were performed by using a Cameca IMS-4f facility with a 12.3 keV O_2^+ primary beam.

III. EXPERIMENT RESULTS

A. Comparative study on the efficiency of radiation damage formation and accumulation

Figure 1 shows fluence dependences of the damage concentration, $n_{da}(N_I)$, formed by 593 MeV Au irradiation of InSb, InP, Ge, GaP, and GaAs at RT. One can see that the irradiation leads to efficient damage formation in InP and especially in InSb. It is worth mentioning that only four ex-

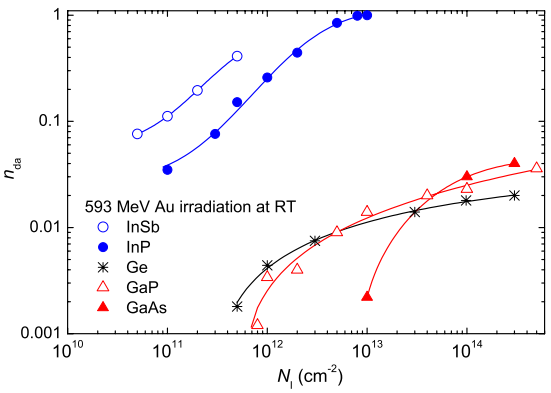

FIG. 1. (Color online) Relative concentration of damage, n_{da}, taken at depth of 200 nm versus ion fluence N_I. The experimental data are for InSb, InP, GaAs, GaP, and Ge irradiated with 593 MeV Au at RT. In all cases the data points can be fitted by sigmoid curves, which are plotted in the figure.

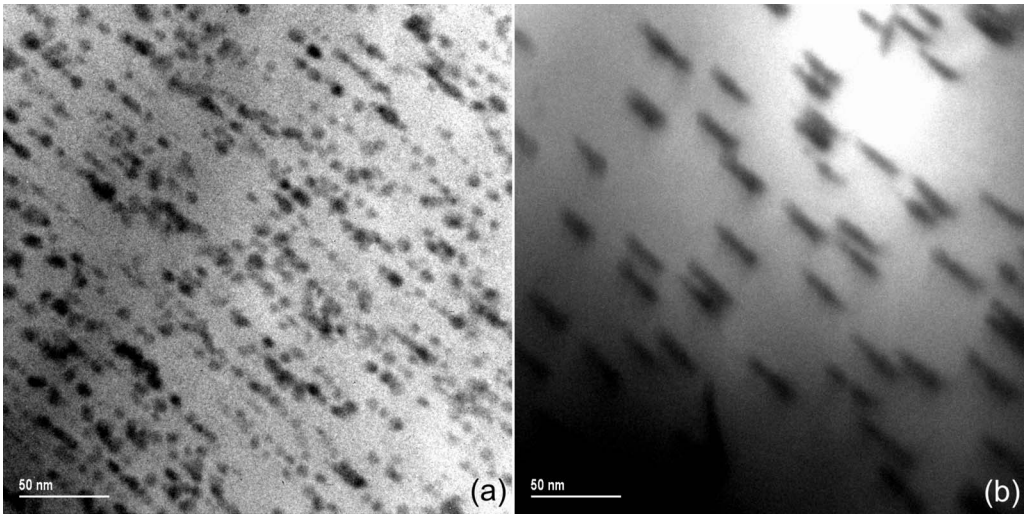

FIG. 2. Bright field PV-TEM images of virgin InP samples irradiated at RT with either (a) 375 MeV Xe up to the ion fluence of 8.4×10^{11} cm^{-2} or (b) 573 MeV Au up to the ion fluence of 1×10^{11} cm^{-2}. In both cases the InP samples were tilted off the ⟨100⟩ axis in the microscope.

perimental data points are presented for InSb in Fig. 1. The reason for that is that at ion fluences above 5×10^{11} cm^{-2} a friable surface layer is formed that can be easily scraped away; therefore, reliable data on n_{da} cannot be retrieved from the respective RBS spectra. We believe that such a modified surface layer stems from a three step process. First, a heavily damaged and partly amorphized surface layer is formed due to large electronic energy deposition by the fast ions. That amorphization is not the final stage of the ion induced lattice damage in InSb in the region of nuclear energy deposition as it was shown nearly 30 years ago.[41] With ongoing irradiation this disordered layer is gradually transformed into a porous layer (as observed previously, e.g., in Ge by Huber *et al.*[42] and in Si by Hedler and co-workers[43,44]). Also in Ge the formation of porous regions was observed after low-energy heavy ion irradiation at high ion fluences (see, e.g., Refs. 45–47). Finally, the thermal outflow of the deposited energy from the surface into the bulk becomes largely hindered due to the presence of the numerous voids. Obviously, this leads to a very efficient heating of the whole surface layer and its thermal decomposition (see, e.g., Ref. 48). In contrast to InP and InSb, the materials Ge, GaP, and GaAs demonstrate much higher radiation resistance, the values of n_{da} for the maximum fluences used are not higher than 0.05, i.e., only 5% of the atoms are displaced from their regular positions in the respective lattices. Therefore, it seems to be impossible to produce high concentration of defects in Ge, GaP, and GaAs by means of fast ion irradiation (see also Ref. 49).

Similar to the case of InP,[50,51] in InSb much less damage is formed due to fast ion irradiations at LNT than at RT. For instance, the damage concentration, n_{da}, formed in InSb due to irradiation with 573 MeV Au up to the ion fluences of 2×10^{11} and 5×10^{11} cm^{-2}, equals about 0.2 and 0.4 at RT and 0.03 and 0.1 at LNT, respectively (not shown).

As it was shown above, different semiconductors exhibit different radiation resistance to fast ion irradiation. Therefore, it is expedient to consider the more sensitive materials separately from the less sensitive ones.

B. TEM results for InP and InSb

Many TEM results on the formation and overlapping of tracks due to fast ion irradiation of InP were already presented previously.[49,51–54] Here only some TEM results on the nature of ion tracks in InP and InSb will be discussed. As an example, Fig. 2 shows ion tracks formed in InP either by 375 MeV Xe or 573 MeV Au irradiation at RT [parts (a) and (b), respectively]. One can see that the ion tracks are discontinuous in the former case and continuous in the latter one.[55] This is in agreement with our calculation results on the ion tracks in InP published previously (see Secs. VII and VIIIB in Ref. 51).

Figure 3 shows two bright field PV-TEM images of ion tracks formed in virgin InSb due to the RT irradiation with 573 MeV Au up to the ion fluence of 5×10^{10} cm^{-2}. The ion tracks are visible either as light spots embedded in the dark (i.e., hardly transparent to the analyzing electron beam) surroundings [part (a) of the figure] or as dark regions [part (b)]. As follows from Fig. 3(a), the surface density of the ion tracks (5×10^{10} cm^{-2}) is in a perfect agreement with the respective value of the ion fluence used. Therefore, in contrast to the much more radiation resistant materials (e.g., GaAs and GaP, see Sec. III C), in the case of InSb each 573 MeV Au ion produces a continuous track at RT. The observed ion tracks are continuous although their diameters are not constant, but vary along their length from about 9 nm to about 18 nm [see Fig. 3(b)]. In contrast, the diameters of tracks visible in Fig. 3(a) are not larger than about 12 nm. Taking further into account the much lower density of the material within the track core as compared to the rest of the track[56] and the irregular shape of the tracks at the entrance/exit surface (not shown), it seems to be very probable that the missing material from the track core is transported in the molten state away toward the surfaces of the thin wedge shaped samples until the track is cooled down due to the heat dissipation. Similar processes were discussed, e.g., in Ref. 57.

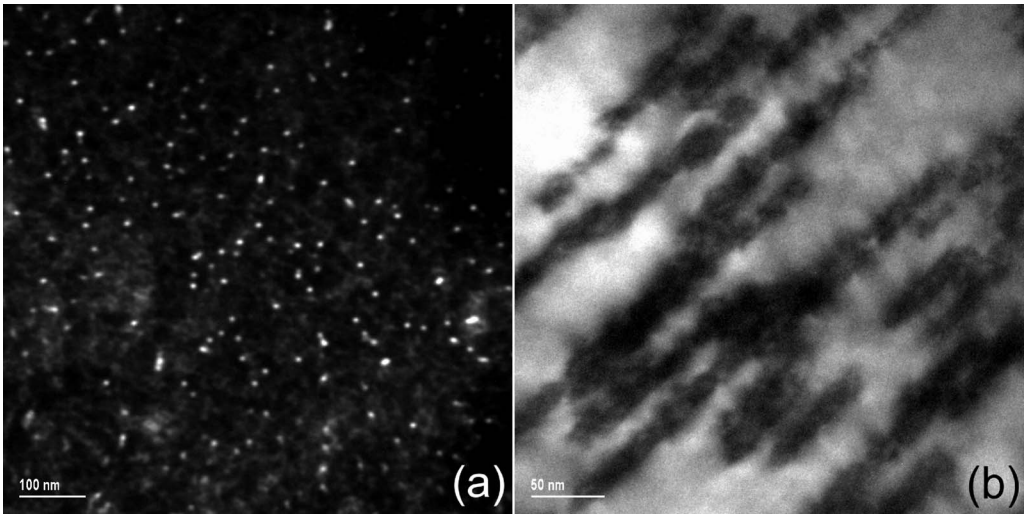

FIG. 3. Bright field PV-TEM images of a virgin InSb sample irradiated at RT with 573 MeV Au up to the ion fluence of 5×10^{10} cm^{-2}. Part (a) was obtained by TEM analysis along ⟨100⟩ direction, while (b) stands for the sample tilted 17° off the axis in the microscope.

C. TEM results for GaAs and GaP

As an example, Fig. 4 shows PV-TEM images of either virgin or predamaged GaAs samples irradiated with 573 MeV Au ions at RT. The ion tracks are visible as local regions having dark contrast (as indicated, e.g., by the dark arrows in the figure). It is worth mentioning that in virgin GaAs [see Fig. 4(a)] only about one of seven ions forms a visible track[58] (cf. the number of tracks of 1.5×10^{11} cm^{-2} and the accumulated ion fluence of 1×10^{12} cm^{-2}). Furthermore, as it follows from the TEM image taken with the same sample but tilted with respect to the analyzing electron beam [Fig. 4(b)], the tracks in virgin GaAs are strongly discontinuous and have a close resemblance to single blobs aligned in the incidence direction of the Au ions (as marked by the dark straight lines in the figure). The surface density of the ion tracks formed due to the 573 MeV Au irradiation at LNT [see Fig. 4(c)] of approximately 7.4×10^{10} cm^{-2} (cf. with the respective ion fluence of 1×10^{12} cm^{-2}) is even lower than that for the RT irradiation. Furthermore, the blobs constituting the ion tracks formed at LNT are shorter and much rarer as compared to the tracks formed at RT (not shown). In contrast to virgin GaAs, in predamaged GaAs [Fig. 4(d)] the number of tracks (4.5×10^{10} cm^{-2}) is very close to the value of the ion fluence used (5×10^{10} cm^{-2}). Taking into account the experimental error in the estimation of the ion fluence (±10%), one can conclude that each 573 MeV Au ion produces a visible track in predamaged GaAs.

Similar to the case of GaAs, the irradiation of virgin GaP with 573 MeV Au at RT leads to the formation of ion tracks (see Fig. 5). Their surface density was found to be equal to about 7×10^{10} cm^{-2} (cf. with the respective accumulated ion fluence of 1×10^{12} cm^{-2}). Furthermore, the off-axis PV-TEM investigations have shown that they are heavily discontinuous (not shown) and that was also the case for GaAs.

D. SIMS results for GaAs and InP

As it was already mentioned in Sec. I, experiments on intermixing of layered structures are potentially capable to

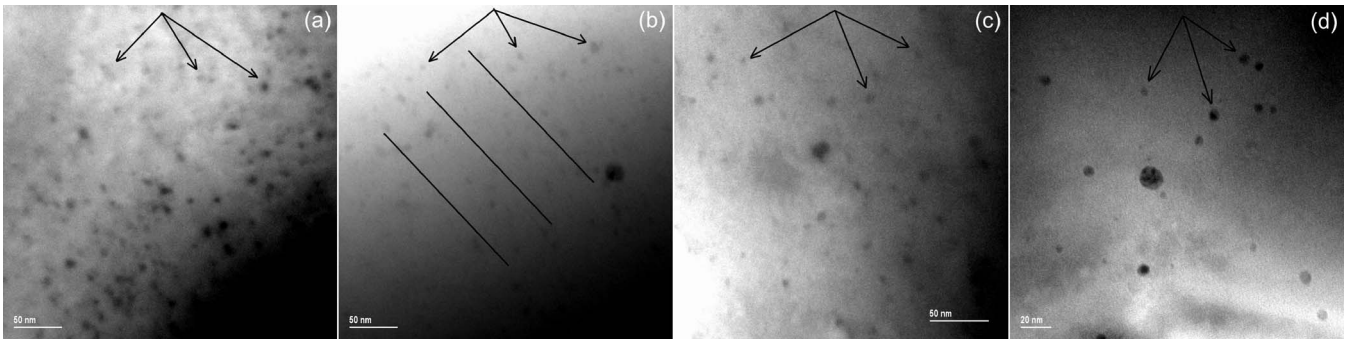

FIG. 4. Bright field PV-TEM images of either virgin (a)–(c) or conventionally predamaged (d) GaAs samples irradiated with 573 MeV Au up to the ion fluences of (a)–(b) 1×10^{12} cm^{-2} at RT, (c) 1×10^{12} cm^{-2} at LNT, and (d) 5×10^{10} cm^{-2} at RT. Parts (a), (c), and (d) were obtained by TEM analysis along ⟨100⟩ direction, while (b) stands for the same sample as shown in (a) but tilted 30° off the axis in the microscope. The dark straight lines in (b) indicate the incidence direction of the Au projectiles. The dark arrows in all parts of the figure indicate some tracks.

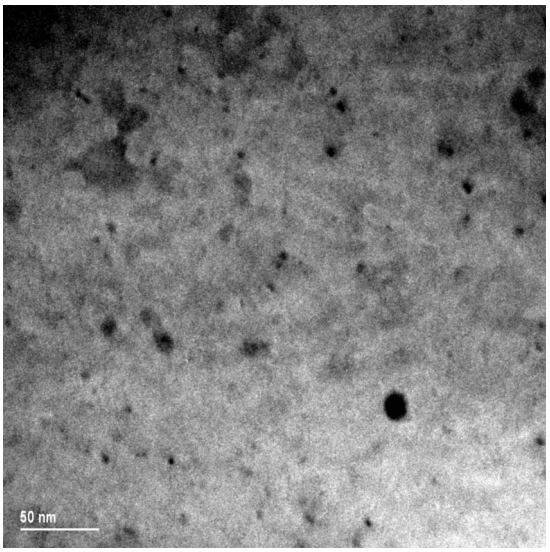

FIG. 5. Bright field PV-TEM image of GaP sample irradiated with 573 MeV Au up to the ion fluence of 1×10^{12} cm^{-2} at RT.

provide an important information on the local melting of the target matter inside SHI tracks. Therefore, Bi/GaAs and Bi/InP layered structures (see Sec. II on details of the sample preparation) were irradiated at RT with 593 MeV Au (5×10^{13} cm^{-2}).

Afterwards, both the unirradiated and SHI irradiated layered structures were investigated by means of the SIMS technique. In all cases the sputtering starts from the Bi layer on the top of the GaAs or InP bulk, respectively. In Fig. 6 the resulting SIMS yields are plotted versus the sputtering time t for Bi/GaAs (upper part) and Bi/InP (lower part). In both parts close to the surface the x coordinates correspond to equal depths because the Bi layers on top of the GaAs or InP have equal properties; particularly, their thickness equals 62 ± 2 nm in both cases, as it was measured by RBS and surface profilometry.[54] From the upper part of Fig. 6 one can see that the irradiation of the Bi/GaAs layered structure almost does not modify the SIMS profiles for both Ga and As constituents. The slight difference between the respective profiles can be explained by the ballistic intermixing[59–62] due to the low but not negligible value of the nuclear energy loss ε_n.

By contrast, in the case of the Bi/InP system the effect of the SHI irradiation is very noticeable. It is quite obvious that In and P atoms are in large quantities transported through the Bi/InP interface toward the surface. This means that unlike the interface between Bi and GaAs, the Bi/InP interface is not so sharp after the SHI irradiation as it was prior to it. If the observed large effect in the Bi/InP system were a result of ballistic intermixing,[59–62] the same large effect should occur in the Bi/GaAs as well because the respective values of ε_n and N_d are very close to each other for InP and GaAs (see Table II). However, this is clearly not the case, as shown from Fig. 6. Thus, the efficient intermixing observed in the case of the Bi/InP layered system cannot be ascribed to the action of the nuclear energy deposition ε_n and, consequently, must be governed by the electronic energy loss ε_e. Taking further into account the observation that both sides of the

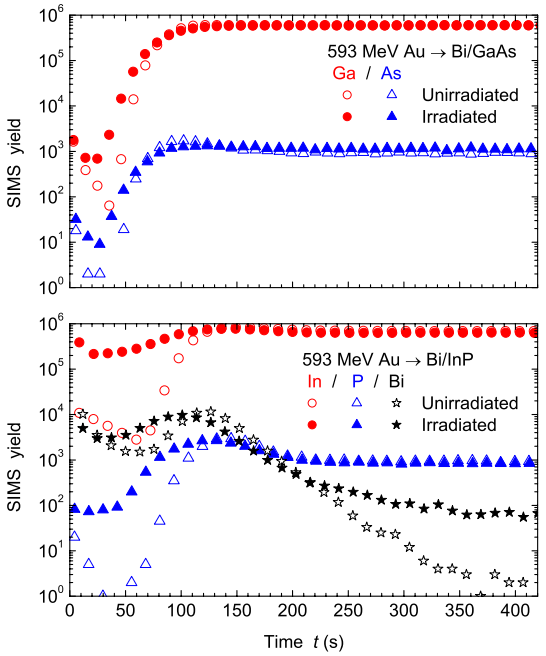

FIG. 6. (Color online) SIMS results on the intermixing in Bi/GaAs and Bi/InP layered structures due to 593 MeV Au irradiation (5×10^{13} cm^{-2} at RT). The upper and the bottom parts of the figure stand for Bi/GaAs and Bi/InP layered structures, respectively. The bottom part shows also the respective profiles of Bi for comparison. The small peaks at the surface (at $t=0$) are inevitably caused by the transitional character of the target sputtering at the very beginning.

interface must be locally molten by SHIs in order to make an efficient intermixing possible (see Sec. I and Refs. 18–20, 22, and 23), one can conclude that the observed large difference between the magnitude of the intermixing in Bi/GaAs and Bi/InP layered systems can be easily understood if assuming that in GaAs, contrary to InP, no molten tracks are formed (alternatively, the ion tracks have negligible dimensions or exist too shortly to cause a noticeable transient interduffusion across the interface Bi/GaAs).

To sum up, the observed difference between GaAs, on the one hand, and InP, on the other hand, is in agreement with the fact that GaAs is much more resistant to SHI irradiation than InP (see Sec. III A).

IV. CALCULATION RESULTS

In our previous paper[51] we presented calculation results on the possibility of track formation in InP due to elemental ions. In this paper the theoretical study is extended toward cluster and elemental ion irradiations of such technologically important semiconductors as Si, Ge, GaAs, and InP.

The available experimental results on the formation of tracks in InP, GaAs, Ge, and Si by cluster ions are summarized in Fig. 7. The figure shows that the irradiation with energetic cluster (C_{20} or C_{60} fullerene) ions leads to the formation of ion tracks provided that the respective electronic energy loss is higher than the threshold of approximately 14, 31, 33, and 37 keV/nm for InP, GaAs, Ge, and Si, respectively. With increasing electronic energy loss, the cross sec-

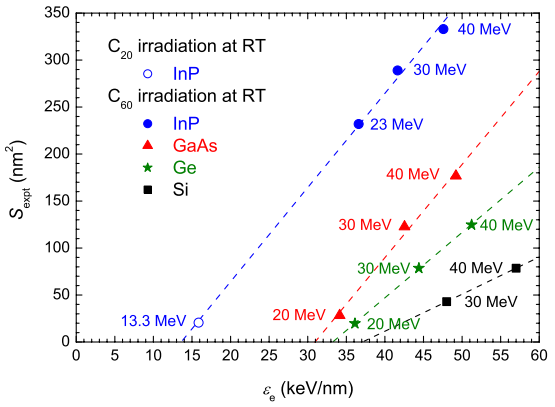

FIG. 7. (Color online) Experimental damage cross section, S_{expt}, versus the electronic energy loss, ε_e, for C_{20} or C_{60} cluster ions. The data on InP are from Refs. 63 and 68, the data on GaAs and Ge are from Refs. 67 and 64, respectively, and the data on Si are from Refs. 65 and 66.

tion of the damaged zones (tracks) increases as well (see Fig. 7). A further important point to mention is the number of ion tracks and specifically the question whether each incident cluster ion forms a (visible) track. A comparison of the value of the ion fluence used with the resulting surface density of the ion tracks in various materials shows that this question can be answered positively for InP,[63] Ge,[64] and Si (Refs. 65 and 66) but not GaAs.[67] In the latter case, as shown in Fig. 1 of Ref. 67, the surface density of the ion tracks formed by C_{60} cluster ions in GaAs is equal to about 4×10^{10}, 5.2×10^{9}, and 3.3×10^{9} cm^{-2} for the beam energies of 20, 30, and 40 MeV, respectively. The corresponding values of the ion fluences used are about 2×10^{12}, 3×10^{11}, and 2.5×10^{11} cm^{-2}, respectively. Therefore, in the case of GaAs the surface density of the visible tracks is more than one orders of magnitude lower than the respective ion fluence used. Hence, GaAs must be first predamaged in order to observe a one to one ratio between the surface density of the ion tracks and the ion fluence used. This finding is in agreement with the TEM results on GaAs (see Sec. III C); furthermore, it is similar to that for InP (see Ref. 53).

In the following the experimental data mentioned above were used for the calculations in the framework of the extended thermal spike model presented in Ref. 51. In order to perform calculations of the thermal spikes due to cluster ions, our program code HEAT (Ref. 51) was slightly modified to take into account the internal structure of the cluster ions. This step is especially important to calculate the spatial distribution of the radiation dose $D(r)$ (i.e., the local energy density) in the matter due to each particular cluster ion. For that, we calculated the Cartesian coordinates (x,y,z) of all constituent atoms in a cluster relatively to its center of symmetry by using the respective data for C_{60} molecules.[70] Furthermore, three-dimensional rotations of the cluster ions were accounted for in the program as well by means of quaternion and matrix operations. It should be mentioned that the "vicinage effects" affecting the stopping of cluster ions in matter (see, e.g., Refs. 71 and 72) were not considered because of their complexity. The dependence of the electron-phonon coupling on the local electronic temperature

TABLE III. Comparison of some intermediate data in the case of irradiation of InP with either elemental ions (390 MeV Xe) or cluster ions (40 MeV C_{60}). The data include the maximum range $R_e^{\max}$ of the detached electrons [calculated with the CASINO code (Ref. 69)], as well as their initial concentration N_e^{init} and the radiation dose at the projectile path [obtained by using our program code HEAT (Ref. 51)]. The data are for the target surface ($z=0$).

Value	390 MeV Xe	40 MeV C_{60}
$R_e^{\max}$ (nm)	160	1.7
N_e^{init} (nm^{-3})	24.1	330
Dose ($\mathrm{keV/nm}^3$)	3.36	44.8

in InP was already presented in our previous paper,[51] and thus only the electron diffusivity D_e remains unknown in the case of cluster irradiations. In order to calculate its value, D_e was first taken arbitrarily and changed until the calculated radii of molten zones, R_{calc}, in InP irradiated with 30 MeV C_{60} ions equaled the radii of the ion tracks known from the recent experiments (Refs. 63 and 68). The resulting value of $D_e=4.65\times10^{-6}$ m^2/s was used for all calculations on cluster irradiations of InP. It is worth mentioning that in the case of C_{60} cluster irradiation the energy is deposited into the target electrons within a much narrower cylindrical region as compared to the case of elemental ions. This is illustrated in Table III where some characteristic values are presented for irradiation of InP with 390 MeV Xe, on the one hand, and 40 MeV C_{60}, on the other hand. Obviously, irradiation of InP with 40 MeV C_{60} leads to a much higher local excitation of the target electrons than that of 390 MeV Xe (see Table III). The last explains well the large difference of about an orders of magnitude between the corresponding track radii in InP due to elemental and cluster-ion irradiation (Refs. 54 and 63), respectively.

Furthermore, the results obtained for InP enabled us to perform calculations of thermal spikes caused by fast cluster-ion irradiation of Ge and Si as well. Here we assumed that the values of D_e in Ge and Si for either elemental or cluster-ion irradiations can be approximated by the corresponding values for InP. Furthermore, we have used the same formula for the efficiency of the electron-phonon coupling, g, as in our previous paper,[51]

$$g=\frac{\pi^2 m_e n_e v_s^2}{6\tau_e T_e}, \tag{1}$$

where m_e is the electron mass, n_e is the volume concentration of the free (detached) electrons, v_s is the sound velocity, τ_e is the mean free time between two successive electronic collisions, and T_e is the electronic temperature. In order to calculate the value of the only unknown parameter in Eq. (1), τ_e, we used one experimental point in Fig. 7 for each material (Ge and Si). The corresponding value of τ_e for each material was at first taken arbitrarily and then changed until the calculated radius of the molten zone, R_{calc}, equaled that of the ion tracks found in the experiments (Fig. 7). The resulting values of τ_e are 4.2×10^{-16} and 1.9×10^{-17} s for Ge and Si, respectively.

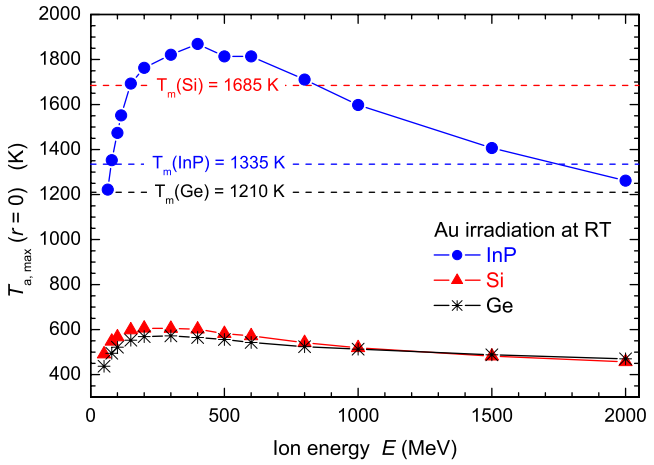

FIG. 8. (Color online) Dependence of the maximum atomic temperature at the ion track axis (r=0) on the energy of fast Au ions. All results are for RT irradiations. The data for InP are from Ref. 51.

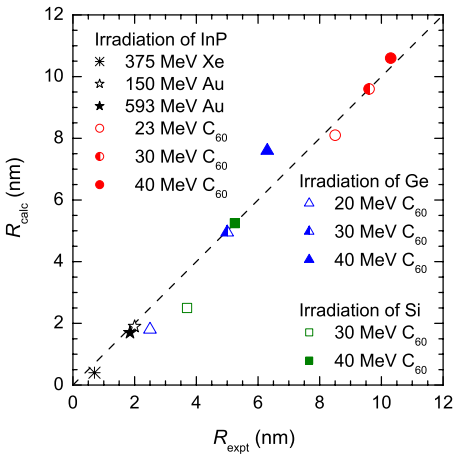

FIG. 9. (Color online) Track radii calculated by our program HEAT (R_{calc}) versus experimental (TEM) values of track radii (R_{expt}) for RT irradiations of InP and Ge with various ion species and energies. The experimental data on the C_{60} cluster-ion irradiations are from Refs. 63, 64, and 68.

After that step one can perform the calculations on irradiation with elemental ions. As it was mentioned above, each C_{60} cluster ion forms a track in InP, Ge, and Si but not in GaAs. That is why we were able to perform the calculations for irradiation with elemental ions in InP, Ge, and Si but not in GaAs. The results of the calculations for the case of RT irradiations with Au ions are presented in Fig. 8. In that figure the calculated maximum atomic temperature (at r=0, where r is the radial distance from the ion path) is plotted versus the energy of Au ions. In all cases the maximum atomic temperature first increases and then gradually decreases with ion energy. The corresponding melting points of InP, Ge, and Si are plotted as dashed lines. One can see that only in the case of InP the maximum atomic temperature exceeds the melting point within a broad range of ion energies. In contrast, this is definitely not the case for both Ge and Si, where the respective maximum values are about 600 K at the most (see Fig. 8). This explains well why no continuous ion tracks were found in crystalline Si and Ge after irradiations with elemental ions but only dotlike heavily discontinuous tracks in Ge (Ref. 73) due to simultaneous stripping of many electrons off the ion (such processes have very low probability[74]).

Figure 9 shows an overview of the calculated track radii, R_{calc}, versus the corresponding experimental ones, R_{expt}, for RT irradiations of InP, Ge, and Si with either elemental or cluster ions. One can see that the calculated values are in good agreement with the experimental ones.

V. DISCUSSION

As it was shown in Sec. III, bombardment of crystalline semiconductors with fast ions leads to the formation of radiation damage. The measured damage concentration, n_{da}, depends primarily on the target material, ion species and energy, and irradiation temperature. In GaP, GaAs, and Ge the respective values of n_{da} are still relatively low (less than 5%) even for the highest ion fluences used (see Fig. 1). Most probably, for these materials the *threshold* value of the *electronic energy deposition* to melt the material along the whole ion tracks is not yet reached with 593 MeV Au ions, which is in agreement with results published by other groups.[75] That means that no continuous tracks can be produced at RT in those materials by fast elemental ions but only heavily discontinuous tracks consisting of small blobs (clusters of defects). This is in good agreement with the TEM results obtained for GaAs and GaP (see Figs. 4 and 5, respectively). Furthermore, because the *electronic energy loss* is thus too low to form heavy damage/tracks in GaP, GaAs, or Ge, the damage production due to the *nuclear energy loss* can become the principal mechanism for such subthreshold regimes, as it was discussed previously.[49,51,76,77] Usually the number of displacements per lattice atom $n_{d\,pa}$ is taken to quantify the nuclear energy deposition with $n_{d\,pa}=N_d N_I/N_a$, where N_d and N_I are the number of displacements per ion and unit path length (see Table II) and the ion fluence, respectively, and N_a is the atomic density of the target (see Table I). For example, in the case of 593 MeV Au irradiation up to the ion fluence of 3×10^{14} cm^{-2}, the value of $n_{d\,pa}$ is thus equal to about 0.23, 0.07, and 0.10 for GaAs, GaP, and Ge, respectively. However, the corresponding measured relative concentration of the damage, n_{da}, does not exceed 0.04 in all three cases, as shown in Fig. 1. This demonstrates that the radiation damage formed due to the elastic stopping in single atomic cascades is not stable. That instability can be explained, e.g., by efficient diffusion and annihilation of point defects or by the damage annealing due to the high electronic energy deposition ε_e.

However, if the studied materials are predamaged prior to the irradiation with fast ions, this obviously makes it easier to produce visible tracks though (see Refs. 51 and 53, and Sec. III C). We believe that the existing disorder (e.g., point defects and point defect clusters) enhances the interaction between electrons excited by fast ions and surrounding atoms, and thus noticeably increases the electron-phonon coupling efficiency g (see Eq. (1)). In this way the energy ini-

tially deposited in the electrons is more efficiently transferred to the lattice (i.e., in terms of the thermal spike model, higher lattice temperature is reached at a fast projectile's path), which obviously facilitates the formation of visible tracks.[51]

In contrast to the much more radiation resistant GaP, GaAs, and Ge, for equal irradiation conditions, a very noticeable amount of radiation damage is produced in InP and InSb (see Fig. 1) in form of point defect clusters and ion tracks due to the high electronic energy deposition ε_e. With increasing ion fluence, more and more radiation damage is formed until complete amorphization of thin surface layers. It is worth mentioning that no significant difference in the atomic structure of InP samples amorphized either due to SHI or conventional ion irradiation was found recently by Schnohr *et al.*[78], despite the fundamentally different energy-transfer mechanisms. The measured concentration of the damage, n_{da}, depends not only on the target material, ion species and energy, and irradiation temperature but also on the ion flux and target doping. Specifically, the RT irradiation with 390 MeV Xe up to the ion fluence of 1×10^{13} cm^{-2} produces in *n*-InP an about 5.5 times larger damage concentration than in *p*-InP (not shown). Furthermore, all other irradiation conditions being equal, in the case of *p*-InP also the magnitude of the ion flux, influences the resulting value of n_{da}. For example, for the RT irradiation of *p*-InP with 390 MeV Xe up to the ion fluence of about 1×10^{13} cm^{-2}, the measured value of n_{da} for the larger ion flux Φ of 3.4×10^{10} cm^{-2} s^{-1} is about 4.5 times larger than that for the lower value of Φ of 2.1×10^{10} cm^{-2} s^{-1} (not shown). In contrast, in the case of 150 and 593 MeV Au irradiations of InP no noticeable influence of the target doping was observed. It should be mentioned in this connection that for both 150 and 593 MeV Au irradiations the corresponding calculated radii of molten ion tracks are relatively large (about 2 nm, see Ref. 51). In contrast, the respective calculated radii of the molten zones in virgin InP irradiated with 390 MeV Xe do not exceed 0.6 nm.[51] Because this value is only slightly larger than the lattice constant of InP (0.587 nm, see Table I), not tracks but rather point defects and point defect clusters are formed at first in virgin InP by fast Xe ions. Therefore, as it follows from the results mentioned above, target doping cannot remarkably influence the efficiency of the damage formation in InP for irradiation conditions where each single ion produces a heavily disordered track with a track radius, which is noticeably larger than the respective lattice constant.

The ion tracks observed in InP and InSb can be either discontinuous or continuous depending on the ion species, ion energy, and irradiation temperature (see Figs. 2 and 3, and Ref. 51). With increasing ion fluence single-ion tracks accumulate and overlap, which finally leads to the formation of amorphous surface layers at large ion fluences.[50,52,53,76] The observed intermittence or quasi-intermittence of the ion tracks can have different nature. In the first basic approach the primary importance is assigned to the well-known dynamic fluctuations of the ion charge due to the electron capture and loss processes (see, e.g., Ref. 74). Those statistical fluctuations of the ion charge are immediately followed by the corresponding fluctuations of the energy loss. Providing that from time to time such fluctuations reduce the momentary value of the energy loss below the respective threshold (minimum) for track formation, discontinuous tracks can be produced in this way. Such discontinuous tracks have no regular structure, as shown, e.g., in Fig. 2(a), because of the statistical nature of the underlying processes. However, providing local melting within the ion tracks, it is also imaginable that the liquid phase is broken into droplets due to the surface tension. Such a process must be particularly facilitated if the material mass density in the liquid state is higher than that in the solid state, which holds for InP, InSb, GaAs, Ge, and Si (see Table I). In that case the observed internal structure of ion tracks must be more regular than in the first case (see above). This is illustrated in Fig. 10 that shows the same sample as in Fig. 2(b) but analyzed in the ⟨111⟩ direction. One can see the regular intermittent structure of the tracks, which was already discussed in Refs. 79 and 80. However, despite that apparent intermittence, a more careful observation shows that the ion tracks depicted in Fig. 10 are still continuous but consisting of regions with lighter and darker contrast.[81]

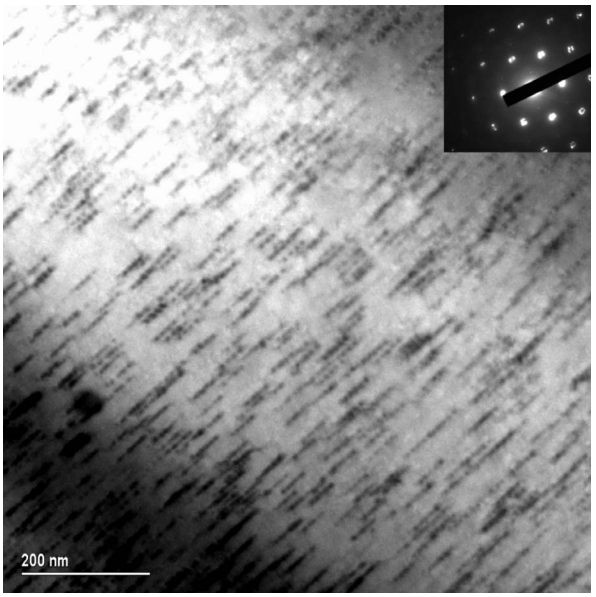

FIG. 10. Bright field PV-TEM image of virgin InP sample irradiated at RT with 573 MeV Au up to the ion fluence of 1×10^{11} cm^{-2}. The TEM analysis was performed in the ⟨111⟩ direction. The inset in the top right corner shows the corresponding diffraction pattern.

As it was described in Sec. IV, the available experimental data on track formation in InP, Ge, and Si due to RT irradiations with C_{60} fullerenes were used in our calculations based on the thermal spike model. Those calculations enabled us to estimate the unknown values of τ_e in Eq. (1) for Ge and Si and thus to perform the respective calculations of the maximum lattice temperature within tracks of fast elemental ions (see Sec. IV). The results obtained by the calculation of the Au irradiations at RT showed that in contrast to InP, in both Ge and Si, the respective maximum lattice temperatures within ion tracks are at the most about 600 K and thus much lower than the melting points of Ge and Si (see Fig. 8). This

explains well why no continuous tracks were found in crystalline Si and Ge after irradiations with elemental ions but only heavily discontinuous ones in Ge.[73]

As it was mentioned in Sec. I, besides the thermal spikes, there are three more competing mechanisms of the damage formation in solids due to high electronic energy deposition, specifically, Coulomb explosion, shock waves, and lattice relaxation (also called athermal melting). However, the experimental results on the above threshold irradiations presented in this paper and elsewhere[51] can be understood only in the framework of the thermal spike model. Particularly, the large influence of the irradiation temperature on the radii and internal structure of visible tracks[51] supports the thermal spike mechanism but contradicts the three others. Also the TEM results on the ion tracks in InSb (Sec. III B) and the SIMS results on the intermixing of the Bi/GaAs and Bi/InP layered structures (Sec. III D) support the idea of the local melting within the ion tracks and, consequently, are a sound argument for the thermal spike model of track formation. Nevertheless, in the case of *subthreshold* irradiations of semiconductors some other mechanisms (presumably, the lattice relaxation mechanism) can become the dominating ones, apart from the processes triggered by the nuclear energy loss.

Such a remarkable difference between InP and InSb, on the one hand, and GaAs, GaP, and Ge, on the other hand, is very intriguing. However, it still remains to be answered why materials with similar properties (cf., e.g., GaAs and InP, see Table I) behave themselves so differently under SHI irradiation. The existing models that try to answer this question are divided into two basic classes. The first class is constituted by the so-called "topological" models that relate the radiation resistance of materials to their respective geometrical structure (e.g., see Ref. 82). The second large class includes various models that relate the resistance to certain physical or chemical properties of materials, such as ionicity, density, elastic moduli, glass forming ability, or melting point (as reviewed, e.g., in Ref. 83). Nevertheless, up to now, no model is able to describe all different materials self-consistently.

VI. SUMMARY AND CONCLUSIONS

Swift heavy ion irradiation of semiconductors leads to the formation of radiation damage in the region of dominating electronic energy deposition. Under identical irradiation conditions, the relative defect concentration n_{da} measured by means of Rutherford backscattering spectrometry differs significantly for the various materials investigated. Whereas in GaP, GaAs, and Ge, the relative defect concentration after elemental ion irradiation at room temperature does not exceed about 5% also at high ion fluences, in InP and InSb the relative defect concentration increases with increasing ion fluence until a continuous amorphous layer is formed. Cross-section transmission electron microscopy (XTEM) observations show that in GaP, GaAs, and Ge heavily discontinuous tracks occur and the track formation is obviously favored if any predamage is produced prior to the fast ion irradiation. On the other hand, in InP and InSb continuous amorphous tracks are formed, the number of which increases with the ion fluence thus leading to the formation of amorphous layers.

Based on our own results and those obtained by other authors for cluster-ion irradiation of InP, GaAs, Ge and Si, the maximum atomic temperature at the ion track axis, as well as the track radii, were calculated in the framework of the thermal spike model. In order to calculate the thermal spikes caused by elemental and cluster ions the electron diffusivity D_e in Ge and Si for either individual or cluster-ion irradiation was approximated by the corresponding values for InP. For the efficiency of the electron-phonon coupling the same formula as previously used for InP was taken, and the only unknown parameter—the mean free time between two successive electronic collisions, τ_e—was determined from the track radii caused by the cluster ions. With this procedure a very good agreement between calculated and measured track radii for InP, Ge, and Si irradiated under various conditions was obtained. The calculations furthermore showed that in contrast to InP, in both Ge and Si, the maximum lattice temperature within the ion tracks is much lower than the respective melting points of Ge and Si. This explains well why no continuous tracks were found in crystalline Si and Ge after irradiation with elemental swift heavy ions but only heavily discontinuous ones.

Summarizing, our results as well as those obtained by other groups on damage formation due to high local electronic energy deposition provide support for the thermal spike model of track formation in semiconductors but contradict the three other competing mechanisms, namely, Coulomb explosion, shock waves, and lattice relaxation. Thus, visible amorphous or heavily damaged ion tracks occur if the electronic energy deposition per ion and unit length exceeds the threshold value for the melting of the corresponding material. This is possible for elemental ion irradiation of InP and InSb but not in Ge and Si (and, probably, also not in GaAs and GaP) where the energy deposition necessary for melting is that high that the melting temperature cannot be reached by elemental ion irradiation. Moreover, at least in InP and GaAs ion tracks can be formed also in a subthreshold irradiation regime if the material is predamaged. This suggests that the existence of point defects and clusters of point defects in the crystal lattice noticeably increases the electron-phonon coupling efficiency, resulting in a more efficient energy transfer to the lattice. Within the thermal spike model this means that for a given electronic energy deposition in the predamaged crystal a higher temperature is reached than in the perfect one.

ACKNOWLEDGMENTS

We thank S. Klaumünzer and A. Hedler for the assistance during the fast ion irradiations and for the helpful discussions, and M. Mans for the deposition of thin surface layers of Bi on GaAs and InP samples. This work was supported by the Deutsche Forschungsgemeinschaft (Contract No. WE 1707/8-1).

*Present address: Belarusian-Japanese Joint Venture "Solar TII," Lagoiski Trakt 22, Mensk 220090, Belarus; kamarou@tut.by; www.solartii.com.
†www.physik.uni-jena.de/~exphys/ionen

[1] R. L. Fleischer, P. B. Price, and R. M. Walker, *Nuclear Tracks in Solids* (University of California, Berkeley, 1975).
[2] R. E. Johnson and W. L. Brown, Nucl. Instrum. Methods Phys. Res. **198**, 103 (1982).
[3] D. Lesueur and A. Dunlop, Radiat. Eff. Defects Solids **126**, 163 (1993).
[4] D. A. Young, Radiat. Meas. **27**, 575 (1997).
[5] Y. Kitazoe, N. Hiraoka, and Y. Yamamura, Surf. Sci. **111**, 381 (1981).
[6] Y. Yamamura, Nucl. Instrum. Methods Phys. Res. **194**, 515 (1982).
[7] I. S. Bitensky and E. S. Parilis, Nucl. Instrum. Methods Phys. Res. B **21**, 26 (1987).
[8] C. C. Watson and T. A. Tombrello, Radiat. Eff. **89**, 263 (1985).
[9] P. Stampfli and K. H. Bennemann, Phys. Rev. B **49**, 7299 (1994).
[10] P. Stampfli, Nucl. Instrum. Methods Phys. Res. B **107**, 138 (1996).
[11] M. Toulemonde, C. Dufour, and E. Paumier, Phys. Rev. B **46**, 14362 (1992).
[12] S. Furuno, H. Otsu, K. Hojou, and K. Izui, Nucl. Instrum. Methods Phys. Res. B **107**, 223 (1996).
[13] C. Dufour, E. Paumier, and M. Toulemonde, Nucl. Instrum. Methods Phys. Res. B **122**, 445 (1997).
[14] G. Szenes, Z. E. Horváth, B. Pécz, F. Pászti, and L. Tóth, Phys. Rev. B **65**, 045206 (2002).
[15] F. Agulló-López, G. García, and J. Olivares, J. Appl. Phys. **97**, 093514 (2005).
[16] F. Dessauer, Z. Phys. **12**, 38 (1923).
[17] F. Seitz and J. F. Koehler, Solid State Phys. **2**, 305 (1956).
[18] W. Bolse and B. Schattat, Nucl. Instrum. Methods Phys. Res. B **190**, 173 (2002).
[19] W. Bolse, Surf. Coat. Technol. **158-159**, 1 (2002).
[20] W. Bolse and B. Schattat, Nucl. Instrum. Methods Phys. Res. B **209**, 32 (2003).
[21] Z. G. Wang, C. Dufour, S. Euphrasie, and M. Toulemonde, Nucl. Instrum. Methods Phys. Res. B **209**, 194 (2003).
[22] W. Bolse, B. Schattat, A. Feyh, and T. Renz, Nucl. Instrum. Methods Phys. Res. B **218**, 80 (2004).
[23] B. Schattat and W. Bolse, Nucl. Instrum. Methods Phys. Res. B **225**, 105 (2004).
[24] T. Som, B. Satpati, P. V. Satyam, D. Kabiraj, Ajay Gupta, and N. C. Mishra, J. Appl. Phys. **96**, 7141 (2004).
[25] S. K. Srivastava, D. K. Avasthi, W. Assmann, Z. G. Wang, H. Kucal, E. Jacquet, H. D. Carstanjen, and M. Toulemonde, Phys. Rev. B **71**, 193405 (2005).
[26] D. W. Palmer, Properties of semiconductors (2006.02) at www.semiconductors.co.uk.
[27] D. Bimberg, R. Blachnik, M. Cardona, P. J. Dean, Th. Grave, G. Harbeke, K. Hübner, U. Kaufmann, W. Kress, O. Madelung, W. v. Münch, U. Rössler, J. Schneider, M. Schulz, and M. S. Skolnick, in *Physics of Group IV Elements and III-V Compounds*, Landolt-Börnstein, New Series, Group III, Vol. 17, Pt. A, edited by O. Madelung and M. Schulz (Springer-Verlag, Berlin, 1982).
[28] O. Pätzold, B. Fischer, and A. Cröll, Cryst. Res. Technol. **37**, 1058 (2002).
[29] O. Pätzold, I. Grants, U. Wunderwald, K. Jenkner, A. Cröll, and G. Gerbeth, J. Cryst. Growth **245**, 237 (2002).
[30] Online archive on physical properties of semiconductors at www.ioffe.ru/sva/nsm/semicond/index.html.
[31] J. P. Biersack and J. F. Ziegler, *The Stopping and Ranges of Ions in Matter* (Pergamon, Oxford, 1985), Vol. 1.
[32] B. Massarani and J. C. Bourgoin, Phys. Rev. B **34**, 2470 (1986).
[33] L. W. Aukerman, Phys. Rev. **115**, 1125 (1959).
[34] R. Bäuerlein, Z. Phys. **176**, 198 (1963).
[35] J. A. van Vechten, in *Handbook of Semiconductors III*, edited by T. S. Mors (North-Holland, Amsterdam, 1980), Vol. 1.
[36] P. M. Mooney and J. C. Bourgoin, Phys. Rev. B **29**, 1962 (1984).
[37] K. Gärtner, Nucl. Instrum. Methods Phys. Res. B **132**, 147 (1997).
[38] C. Dufour, A. Audouard, F. Beuneu, J. Dural, J. P. Girard, A. Hairie, M. Levalois, E. Paumier, and M. Toulemonde, J. Phys.: Condens. Matter **5**, 4573 (1993).
[39] Z. G. Wang, Ch. Dufour, E. Paumier, and M. Toulemonde, J. Phys.: Condens. Matter **6**, 6733 (1994).
[40] Z. G. Wang, C. Dufour, M. D. Hou, G. M. Jin, Y. F. Jin, E. Paumier, and M. Toulemonde, Nucl. Instrum. Methods Phys. Res. B **135**, 265 (1998).
[41] G. L. Destefanis and J. P. Gailliard, Appl. Phys. Lett. **36**, 40 (1980).
[42] H. Huber, W. Assmann, S. A. Karamian, A. Mücklich, W. Prusseit, E. Gazis, R. Grötzschel, M. Kokkoris, E. Kossionidis, H. D. Mieskes, and R. Vlastou, Nucl. Instrum. Methods Phys. Res. B **122**, 542 (1997).
[43] A. Hedler, S. Klaumunzer, and W. Wesch, Nucl. Instrum. Methods Phys. Res. B **242**, 85 (2006).
[44] A. Hedler (private communication).
[45] I. H. Wilson, J. Appl. Phys. **53**, 1698 (1982).
[46] B. R. Appleton, O. W. Holland, J. Narayan, O. E. Schow III, J. S. Williams, K. T. Short, and E. Lawson, Appl. Phys. Lett. **41**, 711 (1982).
[47] I. B. Khaibullin, G. G. Zakirov, M. M. Zaripov, T. Lohneb, L. Pogány, G. Mezey, M. Fried, E. Kótai, F. Pászti, A. Manuaba, and J. Gyulai, Phys. Status Solidi A **94**, 371 (1986).
[48] Jialu Liu and Tingqing Zhang, Appl. Surf. Sci. **126**, 231 (1998).
[49] W. Wesch, A. Kamarou, E. Wendler, A. Undisz, and M. Rettenmayr, Nucl. Instrum. Methods Phys. Res. B **257**, 283 (2007).
[50] A. Kamarou, W. Wesch, E. Wendler, and S. Klaumünzer, Nucl. Instrum. Methods Phys. Res. B **225**, 129 (2004).
[51] A. Kamarou, W. Wesch, E. Wendler, A. Undisz, and M. Rettenmayr, Phys. Rev. B **73**, 184107 (2006).
[52] O. Herre, W. Wesch, E. Wendler, P. I. Gaiduk, F. F. Komarov, S. Klaumünzer, and P. Meier, Phys. Rev. B **58**, 4832 (1998).
[53] W. Wesch, O. Herre, P. I. Gaiduk, E. Wendler, S. Klaumünzer, and P. Meier, Nucl. Instrum. Methods Phys. Res. B **146**, 341 (1998).
[54] A. Kamarou, Ph.D. thesis, Friedrich-Schiller University, 2006.
[55] The maximum length of the tracks visible in the figure is limited by the thickness of the thinnest (transparent to the analyzing beam of electrons) parts of the wedge shaped PV-TEM samples prepared by means of chemical etching mentioned in Sec. II.
[56] Otherwise no light spots were visible in Fig. 3(a).
[57] B. Schattat, W. Bolse, S. Klaumünzer, I. Zizak, and R. Scholz, Appl. Phys. Lett. **87**, 173110 (2005).

[58] Surely, the more discontinuous the ion tracks are, the less physically meaningful is their surface density, because this quantity thus depends on the thickness of the sample that can be analyzed by means of TEM.
[59] R. S. Averback, Nucl. Instrum. Methods Phys. Res. B **15**, 675 (1986).
[60] W. Bolse, Mater. Sci. Eng., A **253**, 194 (1998).
[61] J. Tarus, K. Nordlund, J. Sillanpää, and J. Keinonen, Nucl. Instrum. Methods Phys. Res. B **153**, 378 (1999).
[62] S. Kumar, P. K. Sahoo, R. S. Chauhan, D. Kabiraj, Umesh Tiwari, D. Varma, and D. K. Avasthi, Nucl. Instrum. Methods Phys. Res. B **212**, 238 (2003).
[63] S. Dhamodaran, A. P. Pathak, A. Dunlop, G. Jaskierowicz, and S. Della Negra, Nucl. Instrum. Methods Phys. Res. B **256**, 229 (2007).
[64] A. Colder, O. Marty, B. Canut, M. Levalois, P. Marie, X. Portier, S. M. M. Ramos, and M. Toulemonde, Nucl. Instrum. Methods Phys. Res. B **174**, 491 (2001).
[65] B. Canut, N. Bonardi, S. M. M. Ramos, and S. Della-Negra, Nucl. Instrum. Methods Phys. Res. B **146**, 296 (1998).
[66] A. Dunlop, G. Jaskierowicz, and S. Della-Negra, Nucl. Instrum. Methods Phys. Res. B **146**, 302 (1998).
[67] A. Colder, B. Canut, M. Levalois, P. Marie, X. Portier, and S. M. M. Ramos, J. Appl. Phys. **91**, 5853 (2002).
[68] S. Dhamodaran (private communication).
[69] D. Drouin, A. R. Couture, R. Gauvin, P. Hovington, P. Horny, and H. Demers, Computer code CASINO, version 2.42, 2002 at www.gel.usherbrooke.ca/casino/index.html.
[70] www.wellesley.edu/chemistry/flick/molecules
[71] N. R. Arista, Nucl. Instrum. Methods Phys. Res. B **164-165**, 108 (2000).
[72] S. Heredia-Avalos, R. Garcia-Molina, and N. R. Arista, Europhys. Lett. **54**, 729 (2001).
[73] F. F. Komarov, P. I. Gaiduk, L. A. Vlasukova, A. J. Didyk, and V. N. Yuvchenko, Vacuum **70**, 75 (2003).
[74] H.-D. Betz, Rev. Mod. Phys. **44**, 465 (1972).
[75] The threshold value of ε_e for continuous track formation in Ge was estimated in Ref. 73 to be about 46 keV/nm to 49 keV/nm.
[76] A. Kamarou, E. Wendler, and W. Wesch, J. Appl. Phys. **97**, 123532 (2005).
[77] W. Wesch, A. Kamarou, E. Wendler, and S. Klaumünzer, Nucl. Instrum. Methods Phys. Res. B **242**, 363 (2006).
[78] C. S. Schnohr, P. Kluth, A. P. Byrne, G. J. Foran, and M. C. Ridgway, Phys. Rev. B **77**, 073204 (2008).
[79] A. S. Khalil, D. J. Llewellyn, M. C. Ridgway, A. M. Stewart, A. P. Byrne, and L. T. Chadderton, Microsc. Microanal. **10**, 580 (2004).
[80] A. S. Khalil, L. T. Chadderton, A. M. Stewart, M. C. Ridgway, D. J. Llewellyn, and A. P. Byrne, Radiat. Meas. **40**, 770 (2005).
[81] Thus, the darker regions must be either more damaged or have higher density than the rest of the track according to the first or to the second approach, respectively.
[82] K. E. Sickafus, L. Minervini, R. W. Grimes, J. A. Valdez, M. Ishimaru, F. Li, K. J. McClellan, and T. Hartmann, Science **289**, 748 (2000).
[83] K. Trachenko, J. Phys.: Condens. Matter **16**, R1491 (2004).